nature neuroscience

Rapid and persistent modulation of actin dynamics regulates postsynaptic reorganization underlying bidirectional plasticity

Ken-Ichi Okamoto[1], Takeharu Nagai[2], Atsushi Miyawaki[2] & Yasunori Hayashi[1]

The synapse is a highly organized cellular specialization whose structure and composition are reorganized, both positively and negatively, depending on the strength of input signals. The mechanisms orchestrating these changes are not well understood. A plausible locus for the reorganization of synapse components and structure is actin, because it serves as both cytoskeleton and scaffold for synapses and exists in a dynamic equilibrium between F-actin and G-actin that is modulated bidirectionally by cellular signaling. Using a new FRET-based imaging technique to monitor F-actin/G-actin equilibrium, we show here that tetanic stimulation causes a rapid, persistent shift of actin equilibrium toward F-actin in the dendritic spines of rat hippocampal neurons. This enlarges the spines and increases postsynaptic binding capacity. In contrast, prolonged low-frequency stimulation shifts the equilibrium toward G-actin, resulting in a loss of postsynaptic actin and of structure. This bidirectional regulation of actin is actively involved in protein assembly and disassembly and provides a substrate for bidirectional synaptic plasticity.

The synapse is a highly specialized structure where various signal transduction molecules and their scaffolding proteins are assembled and interact in a hierarchical organization[1]. It is dynamic, rather than static, and is susceptible to bidirectional remodeling according to the intensity of synaptic input. In the CA1 region of the hippocampus, short bursts of synaptic input induce long-term potentiation (LTP) of synaptic transmission, whereas prolonged low-frequency stimulation induces long-term depression (LTD) of synaptic transmission. In past decades, great effort has been made to elucidate the locus of persistent change responsible for long-term plasticity. It is now generally accepted that synaptic plasticity is at least partially a consequence of persistent modification of two aspects of the postsynaptic organization. First, induction of plasticity changes the postsynaptic protein constituents. For example, LTP induction causes a postsynaptic translocation of proteins such as the AMPA receptor and Ca^{2+}/calmodulin-dependent protein kinase type II (CaMKII)[2–5]. Second, plasticity induction alters postsynaptic structure, including the size and number of dendritic spines, a major site of excitatory synapses[6–16]. In this manner, synaptic activity bidirectionally reorganizes both molecular and structural features, and this reorganization, in turn, underlies synaptic plasticity. However, the mechanisms that couple synaptic activity with postsynaptic structural and molecular remodeling are still not well understood.

Here, we investigated the role of actin as a primary regulator of postsynaptic structure and molecular composition. Actin exists in high abundance postsynaptically and serves both as the primary cytoskeletal component of synapses and as an assembly core for various postsynaptic proteins[1,12–22]. Postsynaptic actin is highly motile, with ~85% being exchanged within 2 min[17]. This is due to a constant turnover, or actin treadmill, between two forms—globular (G-) and filamentous (F-) actin—in spine heads, and to a rapid diffusion between the dendritic shaft and spine heads[17]. This indicates that subtle modulation of one leg of the actin treadmill could rapidly disrupt the equilibrium toward either F-actin or G-actin, making this site a compelling substrate for bidirectional plasticity. In fact, reagents that affect the F-actin/G-actin equilibrium affect various aspects of dendritic spines, including shape, number and motility, as well as synaptic transmission and plasticity[10,15,18,21,23,24]. That actin acts as a regulator of the postsynaptic assembly and its consequent function is further corroborated by the established presence of many signal transduction molecules known to regulate actin and its binding proteins within dendritic spines[1,13]. Given these pieces of evidence, it is reasonable to assume that actin is involved in postsynaptic remodeling.

However, the control of actin dynamics by synaptic activity is not well understood. There is no consensus about the direction of the shift in the F-actin/G-actin equilibrium in response to synaptic stimuli. In studies using a fluorescently labeled phalloidin that specifically binds to F-actin or GFP-actin, both increases[10,25] and decreases[14,18,26] in actin abundance have been reported. These studies cannot distinguish whether this is due primarily to a modulation in the F-actin/G-actin

[1]RIKEN-MIT Neuroscience Research Center, The Picower Center for Learning and Memory, Department of Brain and Cognitive Sciences, Massachusetts Institute of Technology, Cambridge, Massachusetts 02139, USA. [2]Laboratory for Cell Function Dynamics, Advanced Technology Development Group, Brain Science Institute, RIKEN, Saitama, 351-0198, Japan. Correspondence should be addressed to Y.H. (yhayashi@mit.edu).

Published online 7 September 2004; doi:10.1038/nn1311

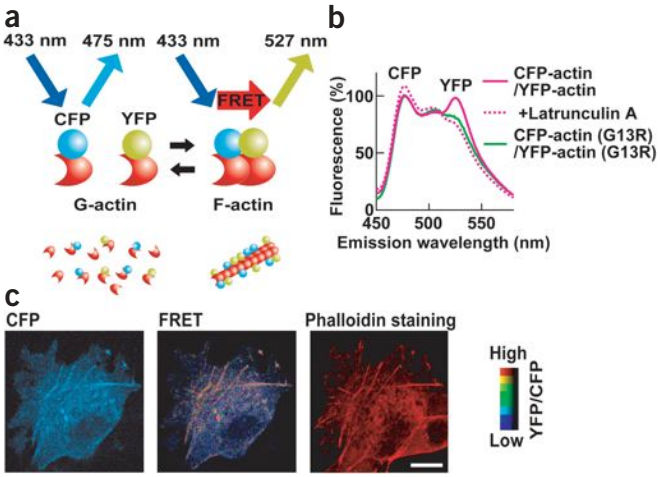

Figure 1 FRET between CFP- and YFP-actin represents F-actin. (**a**) Strategy for detection of F-actin/G-actin equilibrium using FRET (**b**) Emission spectra of HEK293T cell homogenate coexpressing CFP- and YFP-actin before (magenta solid line) and after treatment with 10 μM latrunculin A (magenta dotted line) and of cells expressing G13R mutant CFP- and YFP-actin (green). The homogenate was excited at the CFP specific excitation wavelength of 433 nm. The CFP peak in the absence of latrunculin A was defined as 100%. A YFP peak in cells coexpressing CFP- and YFP-actin was minimized by treatment with latrunculin A or by G13R mutation. (**c**) Images of an NIH3T3 cell transfected with CFP- and YFP-actin and observed under a two-photon laser scanning microscope upon CFP-specific excitation at 800 nm. The CFP image (left) represents the distribution of fluorescent actin. The FRET image (middle) is shown in intensity-modulated display (IMD) mode. Color scale is at right. F-actin (right) was stained with Texas Red–phalloidin after fixation. A high FRET signal (warmer hue) is colocalized with actin filament. Scale bar, 5 μm.

equilibrium or to a consequence of a change in the total amount of actin or the volume of the structure. In addition, the fact that fluorescent phalloidin can be used only in fixed tissue limits the temporal resolution, a crucial parameter for studying synaptic plasticity.

To resolve these issues, we developed an optical approach to measure fluorescence resonance energy transfer (FRET) between actin monomers[27,28] with two-photon laser scanning microscopy in living neurons with single-synapse resolution. This provides the first direct look at the dynamic equilibrium between F-actin/G-actin in intact neurons independent of the total amount of actin, thereby introducing a new parameter to the study of actin dynamics. Using this method, we found that the postsynaptic actin equilibrium modulates rapidly and bidirectionally depending on the frequency of synaptic input. This modulation is sufficient to induce structural changes in spines and synaptic delivery of a representative postsynaptic protein, CaMKII. In this way, the F-actin/G-actin equilibrium represents a previously unidentified locus of persistent modification accompanying synaptic plasticity that bidirectionally reorganizes both postsynaptic structure and molecules.

RESULTS

FRET-based detection of F-actin/G-actin equilibrium

The distance between actin monomers in F-actin is 55 Å, which is within the typical range for FRET (10–100 Å)[27,28]. We therefore proposed that tagging actin with cyan and yellow fluorescent proteins (CFP and YFP) as donor and acceptor, respectively, would allow us

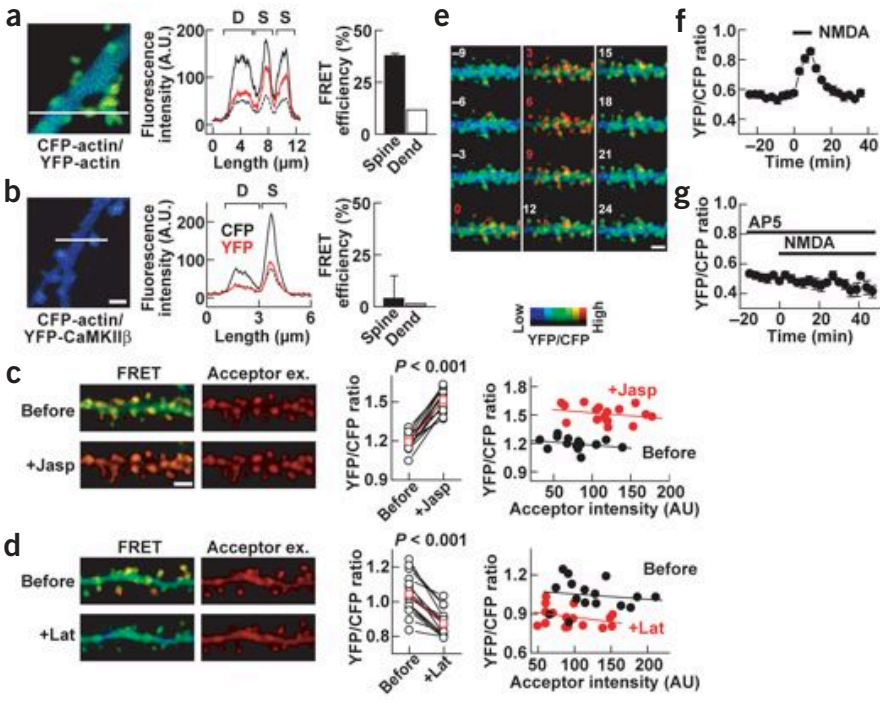

Figure 2 Observation of F-actin/G-actin equilibrium in dendritic spines of CA1 pyramidal cells. (**a**,**b**) FRET images of dendrite expressing CFP- and YFP-actin (**a**) or CFP-actin and YFP-CaMKIIβ (**b**). Middle graphs show fluorescence profiles across the lines. D, dendritic shaft; S, spine; A.U., arbitrary units. Dotted lines are calculated CFP fluorescent profile to indicate leak of CFP into YFP channel. YFP signal above this line is actually derived from FRET. Graphs at right indicate FRET level obtained from acceptor bleaching experiment. Number of spines, 22 for actin and 7 for CaMKIIβ + actin. The data represent four and three independent observations, respectively. (**c**,**d**) Polymerization of actin caused by treatment with jasplakinolide (Jasp; 10 μM, 15 min) and depolymerization with latrunculin A (Lat; 10 μM, 10 min) changes the FRET level. Images of FRET and acceptor at direct acceptor excitation are shown. Middle graphs show FRET level in individual spines (black circles) and average (red squares). Right, spine-by-spine plots of acceptor intensity (integrated through the *z* axis) at acceptor excitation versus FRET level in the presence or absence of drugs. Number of spines, 16 for each drug. The data represent six and four independent observations, respectively. (**e**–**g**) Time-lapse images of a dendrite stimulated (0–10 min) with bath-applied NMDA. FRET was significantly higher between 3 and 18 min after the stimulation ($P < 0.01$). The effect was abolished by DL-AP5 (100 μM). Number of spines, seven without AP5 and six with AP5. The data represent eight and three independent observations, respectively. Numbers in **e** are time stamp in minutes. Scale bars, 2 μm.

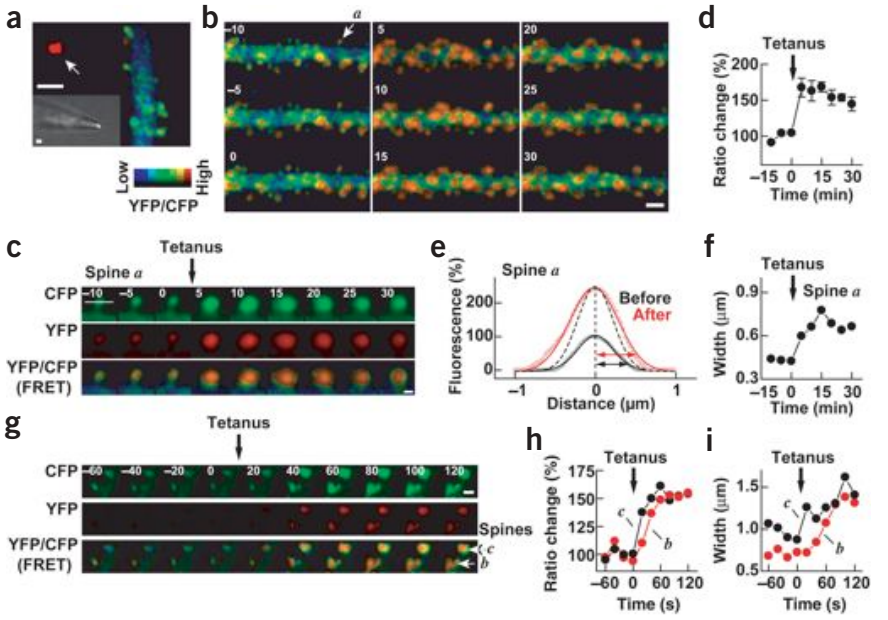

Figure 3 Tetanic stimulation shifts F-actin/G-actin equilibrium toward F-actin and enlarges spine head. (**a**) Configuration of a stimulation. The electrode was loaded with fluorescent beads (arrow) to guide the tip close to the dendritic shaft. Inset, merge of fluorescent and bright-field images. Scale bars, 2 μm. (**b**) Time-lapse images of a dendritic segment captured at 5 min intervals. Tetanic stimulation was applied after image was taken at time 0. Numbers on image are time stamp in minutes. Scale bar, 2 μm (**c**) High-magnification CFP, YFP (at CFP excitation) and FRET images of the spine marked *a* in **b**. Scale bar, 0.5 μm. Numbers are time stamp in minutes. (**d**) The time course of FRET level in six spines from **b**. Average FRET level in individual spines during baseline was taken at 100%. A statistically significant change persisted up to 30 min ($P < 0.01$ as compared with 0 min). Essentially identical results were obtained in 37 cells. (**e**) CFP fluorescence profile of spine *a* across the line in **c**. Open circles represent intensity value at each pixel and solid curves represent Gaussian fits. Black, before stimulation; red, after stimulation. Peak value before stimulation was defined as 100%. Dotted curve represents fluorescence profile before stimulation normalized to the peak after stimulation. Arrows are twice the standard deviation of the Gaussian curve. (**f**) Time course of change in the width of spine *a*. (**g**) Faster time-lapse images of a dendrite taken every 20 s. Numbers are time stamp in seconds. Scale bar, 1 μm. (**h**,**i**) FRET levels (**h**) and width (**i**) of spines *b* and *c* are shown.

to use FRET to observe the equilibrium between F-actin and G-actin in living cells (**Fig. 1a**).

On CFP-specific excitation, the fluorescence emission spectrum of cell homogenate coexpressing CFP- and YFP-actin showed a distinct YFP peak (527 nm) in addition to the CFP peak (475 nm) (**Fig. 1b**). Upon application of the actin depolymerizer latrunculin A, the YFP peak decreased, and this was accompanied by a concomitant dequenching of CFP signal, confirming that the FRET was due to F-actin formation between CFP- and YFP-actin. In contrast, mutations in CFP- and YFP-actin replacing glycine 13 with arginine (G13R), which prevents the formation of F-actin[29], greatly reduced the YFP peak. In addition, two-photon microscopy images of living NIH3T3 cells coexpressing CFP- and YFP-actin revealed incorporation of fluorescent actin in a filamentous pattern generating high FRET levels (as expressed by YFP/CFP ratio throughout). This FRET signal colocalized with F-actin stained with fluorescent phalloidin in the same cell after fixation (**Fig. 1c**).

We then coexpressed CFP- and YFP-actin in CA1 pyramidal neurons in hippocampal slice culture using a biolistic approach. The ratio of YFP to CFP channel fluorescence is consistently higher in dendritic spines than in shafts (**Fig. 2a**). To confirm that this was due to FRET, we calculated the efficiency of FRET by specifically photobleaching the acceptor fluorophore (see Methods for calculation). This showed that FRET actually occurred between CFP-actin and YFP-actin at a higher level in the spines than in shafts. This is consistent with previous experiments in fixed tissue showing accumulated F-actin in spine heads using phalloidin staining[10,14,16,18–20,26]. By contrast, coexpression of YFP-CaMKIIβ, a protein that similarly accumulates at the spine head, and CFP-actin resulted in only very weak FRET, as measured by both YFP/CFP ratio and acceptor bleaching (**Fig. 2b**). This indicates that the FRET is not due to the simple concentration of CFP and YFP at the spine head, but instead to specific interactions between actin monomers.

We next tested whether we could use our FRET system to monitor modulation of the F-actin/G-actin equilibrium. We used two drugs, jasplakinolide and latrunculin A, that are known to shift the equilibrium toward F-actin and G-actin, respectively (**Fig. 2c,d**). Jasplakinolide increased FRET, whereas latrunculin A decreased it, indicating that the current method can detect modulation in both directions. At the same time, these two drugs increased or decreased the total amount of actin at the spine head, as estimated from acceptor (YFP) images taken at direct acceptor excitation, which gives fluorescent intensity independent of the FRET status. We speculated that there might be a positive correlation between FRET signal and total actin content in individual spines. On the contrary, however, the spine-by-spine plot of acceptor intensity at acceptor excitation versus FRET level shows that the FRET value is relatively invariable across spines, although the amount of actin varies significantly. Thus, F-actin/G-actin equilibrium status is not a major determinant of the resting level of actin content. In addition, jasplakinolide and latrunculin shift the overall distribution of the plot, and their effects were similar irrespective of the initial abundance of actin. These results indicate that FRET measures F-actin/G-actin equilibrium independently of total actin amount.

Tetanus shifts F-actin/G-actin equilibrium toward F-actin

To test the effect of NMDA receptor activation on the actin equilibrium, we stimulated neurons by bath applying low concentrations of NMDA (**Fig. 2e–g**). Time-lapse imaging of FRET levels in dendritic spines showed that the F-actin/G-actin equilibrium is relatively constant over time in the absence of the drug. The ratio FRET level was increased by NMDA application, indicating a shift in equilibrium toward F-actin, but after washout it returned to baseline, in a pattern similar to the transient effect of iontophoretically applied NMDA on synaptic transmission[30]. In the presence of the NMDA receptor blocker AP5, the effect of NMDA was eliminated. These results indicate that activation of NMDA receptors can shift the F-actin/G-actin equilibrium toward F-actin. In addition, this shift in actin equilibrium induced by stimulating glutamate receptors lies within the measurable range for our detection system, confirming the utility of our method.

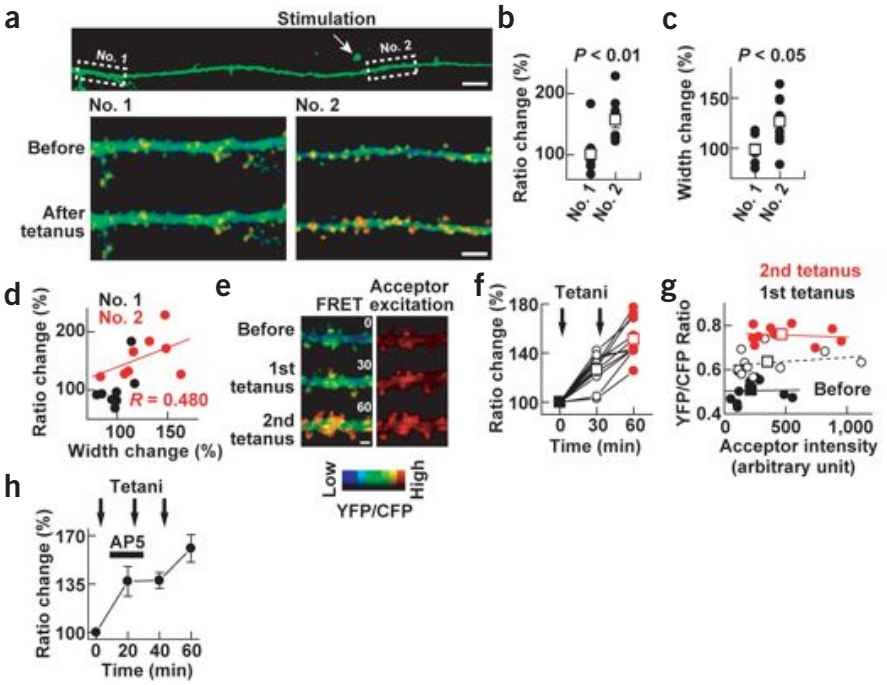

Figure 4 FRET change induced by tetanic stimulation is localized and mediated by synaptic activation of NMDA receptor. (**a**–**d**) Tetanus-induced change in FRET is restricted to the vicinity of stimulation. (**a**) Top, low-magnification image of a dendrite. Area 2 was stimulated. Bottom, FRET images of two dendritic segments taken before and 5 min after tetanic stimulation. Scale bars, 20 μm for top, 5 μm for bottom. Change in FRET level (**b**) and width (**c**) of eight spines from the two areas. Black circles are individual spines and white squares are averages. (**d**) Width change versus FRET change in individual spines. Line, linear fit for the spines in area 2. (**e**) Effect of multiple tetani. FRET and acceptor images before, 30 min after the first and 30 min after the second tetanus are shown. Numbers are time stamp in minutes. Scale bar, 2 μm. (**f**) FRET changes after the first and second tetani, with the level before tetanus defined as 100%. Symbols are as in **b**. (**g**) The same data set plotted versus the amount of actin, estimated from acceptor intensity at acceptor excitation. Values before stimulation and after the second tetanus differed significantly; $P < 0.001$ for FRET and $P < 0.01$ for acceptor intensity. Number of spines, ten. (**h**) Effect of NMDA receptor blockade on tetanus-induced FRET change. DL-AP5 (100 μM) was infused after the first tetanus. Values for adjacent time points were significantly different ($P < 0.001$) in the absence but not ($P > 0.05$) in the presence of AP5. ($n = 13$.)

Next, we synaptically stimulated the neurons by providing tetanic stimulation to the presynaptic fibers through a glass electrode placed near the dendrite (**Fig. 3a**)[2,5], which caused FRET levels in dendritic spines to increase significantly (**Fig. 3b–f**). This increase persisted for at least 30 min after tetanus, in contrast to the response to bath-applied NMDA, which quickly returned to baseline after washout (**Fig. 2e,f**). The onset of the FRET signal increase was rapid. Images obtained at 20-s intervals indicated that the increase began within 20 s after the tetanic stimulation and achieved maximal level after about 1 min (**Fig. 3g–i**).

To monitor the spatial distribution of spines undergoing changes in FRET level, we alternately imaged two dendritic segments of the same neuron, one close to the stimulation electrode and the other ~200 μm away (**Fig. 4a–d**). In spines close to the stimulation electrode, the FRET signal increased after tetanic stimulation. In contrast, there was no obvious change to spines at the more distant location, indicating that the change in the FRET signal is the result of local synaptic activity rather than neuron-wide signaling such as action-potential generation.

We next questioned whether a single tetanus saturated the change in FRET, by subjecting the same dendritic segment to a second tetanus (**Fig. 4e–g**). This further increased FRET levels, showing that the shift in the F-actin/G-actin equilibrium occurs in a graded manner—unlike synaptic response, which shows potentiation an in all-or-none fashion[31]. To test for correlation between the amount of actin present and the magnitude of change in FRET levels at a given spine, we plotted the acceptor intensity at acceptor excitation (considered

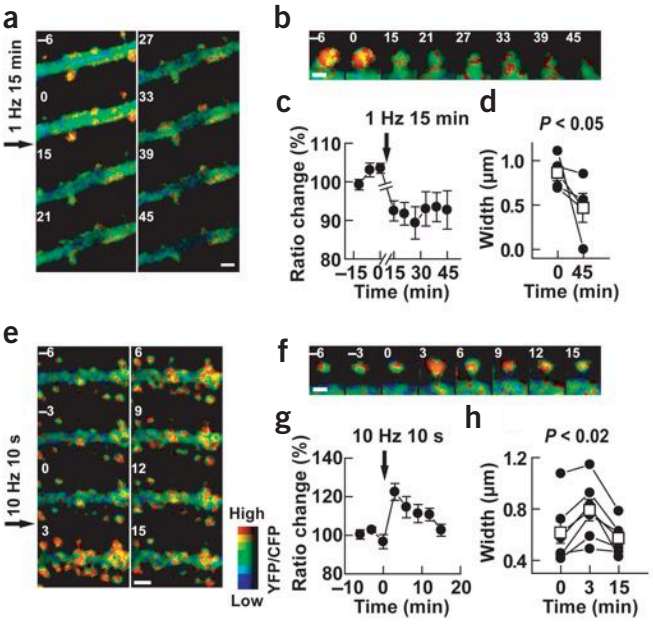

Figure 5 Prolonged low-frequency stimulation induces depolymerization of actin and shrinkage of the spine head. (**a**,**b**) Time-lapse images of a dendritic segment that received prolonged low-frequency stimulation (1 Hz, 15 min) typical of LTD induction. Stimulation was initiated immediately after the image at time 0 was taken and ended before the image at time 15. (**c**) Time course of the FRET signal. Values at time 0 and 30 min after stimulation differed significantly; $P < 0.05$. $n = 4$. (**d**) Plot of spine width before and after low-frequency stimulation. $n = 4$. (**e**,**f**) Time-lapse images of a dendritic segment receiving intermediate-frequency stimulation (10 Hz, 10 s), which typically neither potentiates nor depresses synaptic transmission. (**g**,**h**) FRET level and spine width ($n = 6$ for each) both increased transiently after stimulation and then returned to baseline. The FRET signal was significantly greater at 3 and 6 min after the stimulation ($P < 0.01$) than at 0 min, but thereafter the difference became insignificant ($P > 0.05$). Scale bars, 2 μm for **a**,**e**, 1 μm for **b**,**f**. Numbers are time stamps in minutes. Symbols are as in **Figure 4b**. The results shown for 1-Hz and 10-Hz stimulation are each representative of ten independent experiments with similar results.

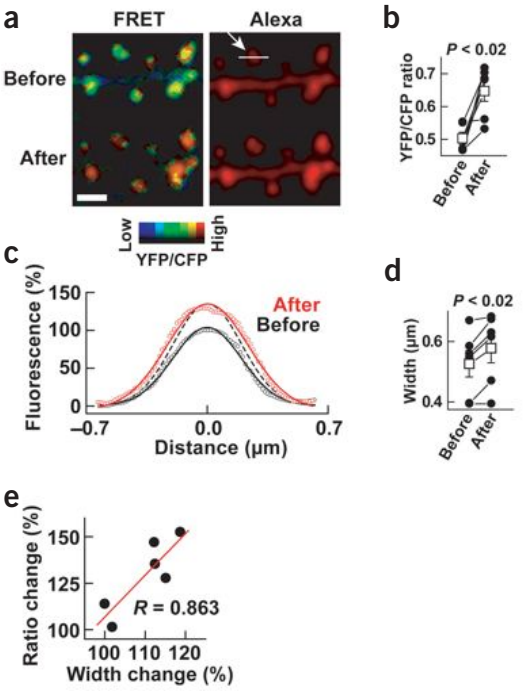

Figure 6 Imaging of cytosolic fluorescence confirms enlargement of the dendritic spine as a result of tetanic stimulation. To monitor structural changes independent of actin redistribution, a neuron coexpressing CFP- and YFP-actin was injected with Alexa 594 and given tetanic stimulation. (**a**) FRET and Alexa 594 images taken before and 5 min after the tetanic stimulation. Scale bar, 2 μm. (**b**) Quantification of FRET in six spines before and after tetanic stimulation. FRET increased in five of six spines. Symbols are as in **Figure 4b**. (**c**) Alexa 594 fluorescence profile of a spine across the line in **a**. Symbols are as **Figure 3e**. (**d**) Width of six spines before and after tetanic stimulation. (**e**) Plot of FRET change versus width change, showing positive correlation. A representative datum from three independent experiments is shown.

proportional to the amount of actin) versus the change in FRET level after tetanic stimulations (**Fig. 4g**). Although the acceptor fluorescence intensity varies significantly across spines, the tetani changed FRET levels in most of them and there was no clear correlation between initial actin content and FRET signal change. At the same time, more actin accumulated in spine heads with each tetanus, indicating a net increase in F-actin content by tetanic stimulation.

The increase in FRET levels after tetanus was blocked by AP5, indicating that it required NMDA receptor activation (**Fig. 4h**). However, after washout of AP5, another tetanus could increase FRET. These results demonstrate that tetanic stimulation rapidly and persistently shifts the F-actin/G-actin equilibrium toward F-actin in an NMDA receptor–dependent manner.

Frequency-dependent modulation of F-actin/G-actin equilibrium

We next applied a low-frequency (1 Hz) stimulation paradigm, which typically induces LTD (**Fig. 5a–d**). After 1 Hz stimulation, we observed a reduction in the FRET that persisted 30 min after the stimulation was stopped. This indicates that, in contrast to tetanic stimulation, a prolonged low-frequency stimulation induces a shift in the F-actin/G-actin equilibrium toward depolymerization. Next we applied a 10 Hz stimulation, an intermediate frequency that typically does not cause either LTP or LTD (**Fig. 5e–h**). Immediately after the stimulation, we observed a transient increase in FRET, which then returned to baseline. These observations indicate that the F-actin/G-actin equilibrium can be regulated bidirectionally in accordance with synaptic plasticity.

Remodeling of dendritic spines by modulation of actin

We next examined the structural consequences in spines of shifting the actin equilibrium. Tetanic stimulation resulted in rapid enlargement of the dendritic spine heads, beginning less than 40 s and persisting up to 30 min after stimulation (**Fig. 3c,f,g,i**). This effect was limited to the vicinity of stimulation and was not observed in distant dendritic segments, much like for the FRET change (**Fig. 4c**). A plot of FRET change versus width change in each spine showed a positive correlation between the two (**Fig. 4d**). Spines that did not show FRET change also did not show any change in width.

To test whether we could observe similar enlargement when we imaged the actual spine structure, rather than the distribution of fluorescent actin, we injected the soluble fluorophore Alexa 594 into neurons and sequentially imaged FRET and Alexa 594 (**Fig. 6**). Consistent with the results obtained with CFP-actin, width measurements (**Fig. 6c,d**) confirmed a significant enlargement in the size of spine heads after tetanic stimulation. Again, the changes in width and in the FRET signal of individual spines were positively correlated, suggestive of a causal relationship between spine enlargement and the shifting of the F-actin/G-actin equilibrium toward F-actin formation (**Fig. 6e**).

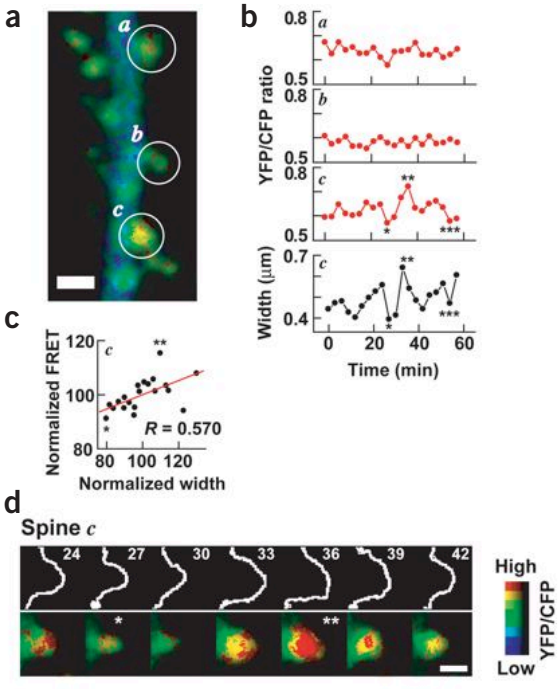

Figure 7 Spontaneous dynamics of dendritic spines are coupled with modulation of actin equilibrium. (**a**) A dendritic segment of a neuron expressing CFP-actin and YFP-actin. Scale bar, 2 μm. (**b**) The FRET level of spines *a–c* (circled in **a**) during a 1-h observation period. Bottom is width of spine *c*. The FRET level in individual dendritic spines was relatively stable (spines *a* and *b*). In one spine (*c*), however, we observed transient decreases (*, ***) and increase (**) in FRET level. These were accompanied by shrinkage (*, ***) and enlargement (**) of the spine head. (**c**) FRET versus width, both normalized to the mean, showing a positive correlation. (**d**) Higher magnification of spine *c*. Top, contour drawing. Scale bar, 1 μm. Numbers are time stamps in minutes.

In contrast, a prolonged 1 Hz stimulation that shifted the equilibrium toward G-actin resulted in a reduction in spine head size (**Fig. 5a**,**b**,**d**). Some spines even disappeared completely after stimulation. A 10 Hz stimulation caused a transient enlargement immediately after the stimulation, which then returned to baseline level (**Fig. 5e**,**f**,**h**). This temporal pattern of size changes matches well with the pattern of change in FRET under this stimulation paradigm (**Fig. 5g**). These results provide further evidence that the modulation of the equilibrium between F-actin/G-actin regulates spine size.

In addition to these stimulus-evoked structural reorganizations, previous reports indicate that the enlargement and shrinkage of dendritic spines can occur spontaneously, without external stimulation[15,32]. We were therefore interested in observing the F-actin/G-actin equilibrium during such intrinsic changes (**Fig. 7**). The spine denoted as *c* (**Fig. 7a**) underwent spontaneous shrinkage and enlargement during 1 h of observation (**Fig. 7b–d**). Comparison of width and FRET level over time showed good temporal correlation between structural and FRET changes. When the spine shrank, FRET decreased, and when the spine enlarged, FRET increased. These were isolated events restricted to spine *c*; other spines (such as spines *a* and *b*) did not show synchronous changes. This observation provides further evidence for the involvement of local modulation of the F-actin/G-actin equilibrium in the regulation of structural characteristics of dendritic spines.

These structural changes were mimicked by pharmacological induction of actin polymerization by bath application of the F-actin stabilizer jasplakinolide or depolymerization caused by latrunculin A, which led to enlargement and shrinkage, respectively, of spine heads (data not shown; see refs. 18,20). This result indicates that the structural changes we observed were a direct consequence of actin polymerization or depolymerization. In sum, our results indicate that bidirectional synaptic plasticity, both positive and negative, is accompanied by enlargement or shrinkage of the spine head, as a result of an input frequency–dependent shift in the F-actin/G-actin equilibrium.

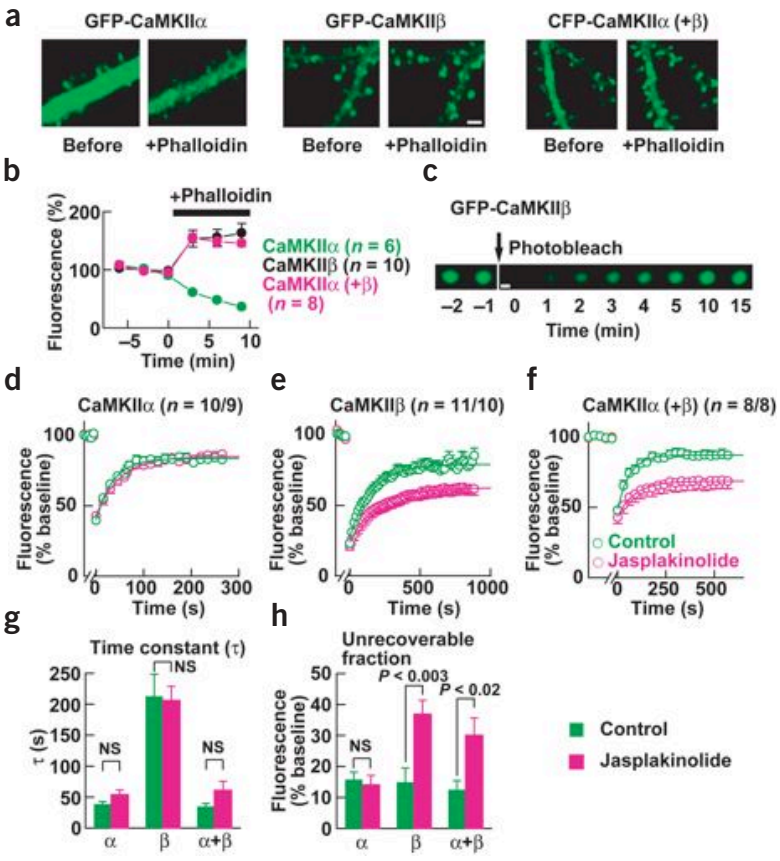

Figure 8 Pharmacological induction of F-actin is sufficient to induce synaptic delivery of CaMKII by increasing postsynaptic binding capacity. (**a**) Images of neurons expressing GFP-CaMKIIα, GFP-CaMKIIβ, and CFP-CaMKIIα coexpressed with YFP-CaMKIIβ captured before and after injection of phalloidin through a whole-cell pipette. Scale bar, 2 μm. (**b**) Time course of fluorescence in spine head before and after phalloidin injection. The formation of F-actin caused an accumulation at dendritic spines of CaMKIIβ but not CaMKIIα, which was gradually lost, most probably owing to wash-out into the whole-cell pipette. But CaMKIIα coexpressed with the β isoform was delivered to dendritic spines by F-actin formation. Fluorescence at time 0 and 10 were significantly different: for CaMKIIα, $P < 0.05$; CaMKIIβ, $P < 0.01$; CaMKIIα + β, $P < 0.02$. Numbers of spines are indicated. (**c**–**h**) FRAP analyses of the effect of actin polymerization on the dynamics of CaMKII subunits. Kinetics were compared in the presence or absence of a cell permeable F-actin stabilizer jasplakinolide (10 μM). (**c**) Time-lapse images of a dendritic spine expressing GFP-CaMKIIβ before and after photobleaching. Scale bar, 0.5 μm. (**d**–**f**) Ensemble data of FRAP analyses of GFP-CaMKIIα (**d**), GFP-CaMKIIβ (**e**) and CFP-CaMKIIα coexpressed with YFP-CaMKIIβ (**f**) in the presence and absence of jasplakinolide. Numbers indicate number of spines analyzed with and without the drug. Only the CFP channel was analyzed in **f**. Recovery time course was fitted to single exponential curve and the time constant (τ) (**g**) and the proportion of fluorescence that did not recover at $t = \infty$ (**h**) were calculated.

Actin increases synaptic CaMKII by increasing binding capacity

Another important aspect of postsynaptic F-actin is its role as postsynaptic scaffold. Therefore, dynamic modulation of F-actin/G-actin equilibrium may serve as an active regulator of postsynaptic binding capacity, thereby contributing to the redistribution of postsynaptic proteins. To explore this, we induced actin polymerization by injecting phalloidin into the neurons and monitored the subsequent redistribution of postsynaptic proteins. The use of phalloidin was designed to isolate the effect of actin polymerization from other signaling cascades, which would be activated simultaneously if tetanic stimulation were used to trigger polymerization.

We first tested the GFP-fusion protein of CaMKIIβ subunit because it is enriched postsynaptically and binds directly with F-actin[33]. Consistent with this, GFP-CaMKIIβ was observed in spine heads under basal neuronal activity. Upon induction of actin polymerization, the abundance of GFP-CaMKIIβ at dendritic spines increased rapidly (**Fig. 8a**,**b**). To test whether this depended on direct binding with F-actin, we imaged GFP-CaMKIIα, because the α isoform does not bind directly to actin but has a domain structure otherwise similar to that of CaMKIIβ. In contrast to that of GFP-CaMKIIβ, the fluorescence of GFP-CaMKIIα was gradually lost after phalloidin injection, most probably owing to washout into the whole-cell pipette (**Fig. 8a**,**b**). However, when CFP-CaMKIIα was coexpressed with CaMKIIβ, it was delivered

to the synapse by actin polymerization, most probably through a hetero-oligomerization with β isoforms. This showed that CaMKIIβ redistribution is a specific result of F-actin formation rather than a secondary effect of volume increase or the formation of a diffusion barrier, as these would affect both α and β isoforms equally.

We next tested whether this effect of actin polymerization was mediated by an increase in postsynaptic scaffold capacity or by an increase in the propulsive force enabling transport into the spine head[34]. To distinguish these two possibilities, we conducted a fluorescence recovery after photobleaching (FRAP) assay[17]. In this assay, the fluorescence of small region, such as the spine head, is photobleached and the recovery of the fluorescence is monitored. In the case of a protein that has no capacity for binding to the spine head, such as free GFP, the fluorescence level typically recovers in an exponential fashion and becomes fully restored to its original level. However, if a population of protein is tightly bound to the spine head, recovery is partial, leaving an unrecoverable fraction. Therefore, an increase in the binding capacity within the spine head would be reflected by an increase in the unrecoverable fraction. In contrast, an increase in transport into the spine head would be reflected as a facilitation of recovery speed, observed as a reduction of the time constant.

We first tested the effects of jasplakinolide in a FRAP assay of GFP-actin. The drug treatment markedly increased the unrecoverable fraction, indicating an increase in the amount of actin tightly bound to the spine head—a result consistent with a shift in the F-actin/G-actin equilibrium toward F-actin (data not shown; see ref. 17). We then conducted the FRAP experiment with α and β isoforms of CaMKII in the presence or absence of jasplakinolide (**Fig. 8c–h**). In control spines, the unrecoverable fraction of GFP-CaMKIIα was 15.8 ± 2.4% of the baseline level and time constant (τ) was 38.7 ± 3.9 s (**Fig. 8d,g,h**). The jasplakinolide affected neither the unrecoverable fraction nor the time constant, consistent with an unaltered distribution of CaMKIIα by jasplakinolide. In contrast, jasplakinolide increased the unrecoverable fraction of CaMKIIβ in spine heads (**Fig. 8e,h**). The recovery speed, however, was not statistically different in the presence of jasplakinolide (**Fig. 8e,g**), ruling out facilitation of transport into dendritic spines. The hetero-oligomer of CFP-CaMKIIα and YFP-CaMKIIβ behaved similarly to CaMKIIβ (**Fig. 8f–h**). Together, these data indicated that polymerized actin increases the amount of CaMKII by providing more binding capacity in the spine but not by facilitating movement of CaMKII molecules.

DISCUSSION

FRET between actin monomers represents F-actin

A previous attempt to monitor the F-actin/G-actin equilibrium used purified and chemically labeled fluorescent actin *in vitro* and observed FRET between actin monomers[27]. This FRET is due to intrafilament, rather than interfilament, alignment of donor and acceptor actin, and its efficiency does not depend on filament concentration, providing an ideal system to detect actin equilibrium in a structure where actin distribution is heterogeneous. We updated this strategy by using genetically encoded fluorescent actins and showed that we can thereby use FRET to monitor the actin equilibrium in living tissue. This provides information about the equilibrium level between F-actin/G-actin. Fluorescently labeled phalloidin stains only F-actin, providing no information about G-actin. A GFP fusion protein of actin has been used to determine the cellular distribution and dynamics of actin in living tissue, but this cannot distinguish the two forms of actin. Thus, the information obtained with our current technique is unique.

This method does have certain limitations. The FRET value, obtained by measuring either acceptor bleaching or the ratio of CFP to YFP intensity, does not give the absolute ratio of F-actin to G-actin. This is because the FRET efficiency depends on the relative levels of donor actin, acceptor actin and endogenous unlabeled actin[27]. The inclusion of unlabeled actin in a filament decreases the chance that donor and acceptor will be aligned within the effective distance. In contrast, an excess of acceptor actin as compared to donor actin increases the chance that the acceptor will be next to the donor, thereby increasing the FRET level while decreasing the overall signal intensity. Because of this limitation, we always took baseline images and limited our comparisons to spines in the same dendrite.

Structural and molecular postsynaptic remodeling by actin

We found that F-actin/G-actin equilibrium is relatively invariable across spines with different amount of actin and is stable under basal neuronal activity (**Figs. 2c,d** and **7**). But this equilibrium can be modulated, both positively and negatively, by a transient synaptic activity (**Figs. 3–6**). This modulation is rapid—it can change within 20 s—and persistent up to at least 30 min. Its bidirectionality depends on the frequency of synaptic input, reminiscent of the Bienenstock-Cooper-Munro (BCM) curve of synaptic plasticity: a short burst of activity induces LTP, prolonged low-frequency activity induces LTD, and intermediate frequencies elicit a neutral response[35,36]. This explains the contradictions between past studies with respect to the behavior of actin in different preparations under various stimulation protocols[14,18,25,26]. The modulation was dependent on NMDA receptor activation. These parallels between synaptic plasticity and actin polymerization status strongly suggest that actin polymerization is an important determinant of the size of synaptic transmission, making it an ideal substrate for the long-term modification underlying long-term synaptic plasticity.

Because actin is the primary cytoskeletal element in the spine head, it is reasonable to imagine that postsynaptic actin polymerization or depolymerization underlies the structural remodeling of spine heads[6–16]. Our observations of changing spine structure in conjunction with a shifting actin equilibrium following plasticity induction establishes strong support for this concept; actin polymerization was accompanied by enlargement of the spine head, whereas depolymerization was accompanied by shrinkage. Because the pharmacological induction of actin polymerization and depolymerization mimicked these structural changes, it is likely that actin polymerization and depolymerization are the primary cytoskeletal mechanisms underlying these changes. The finding that spine size can be enlarged by the same stimulation that induces synaptic plasticity implies that the size of the spine head may represent the history of plasticity of a synapse.

A close correlation between the size of spines and synaptic contact, as well as glutamate receptor density, has been noted[37–39]. Given these correlations, a structural change must be linked with the translocation of postsynaptic proteins. Actin is an ideal mechanism for this process as well because it can also serve as a scaffold for other postsynaptic proteins. Our results indicate that increased postsynaptic F-actin provides increased binding capacity, thereby trapping CaMKII at synaptic sites. Through direct or indirect interaction with F-actin, this mechanism provides a reasonable explanation for the assembly of many different postsynaptic proteins without the need to postulate trafficking signals specific to each protein.

We speculate that this mechanism works synergistically with other mechanism proposed for synaptic plasticity, such as persistent kinase activation[40,41], to maintain enhanced transmission at different times after the induction of plasticity. For instance, AMPA receptor subunits require direct phosphorylation for targeting to the synapse, but this alone is not sufficient for translocation[42]. CaMKII trafficking is also regulated by phosphorylation in addition to the actin-based mecha-

nism described here[4]. Yet actin polymerization by itself is necessary, but not sufficient, to induce synaptic potentiation[10,23,24]. These facts indicate that additional cellular signaling is necessary to link the increase in F-actin to enhanced AMPA receptor–mediated synaptic transmission. Because actin polymerization does not require new protein synthesis, it may explain the 'synapse tagging' effect of synaptic plasticity, whereby newly synthesized molecules necessary for late-phase of LTP affect only the synapse undergoing the synaptic plasticity[43].

In contrast, prolonged low-frequency stimulation shifts the actin equilibrium toward G-actin and a loss of spine structure, which is likely to result in the loss of postsynaptic cytoskeletal integrity, compromising the proteins anchored to it. AMPA receptors are anchored postsynaptically via the actin cytoskeleton, and actin depolymerization is a prerequisite for ligand-induced internalization of these receptors, a proposed mechanism for LTD[20,21,44]. This argues that the shift in actin equilibrium in favor of G-actin and the resultant disruption of the AMPA receptor scaffold trigger LTD. This mechanism may work in conjunction with other proposed mechanisms for LTD, such as those involving phosphatase activation[45] and clathrin-dependent AMPA receptor internalization[44].

Molecular mechanism leading to persistent actin polymerization

Bath application of NMDA was sufficient to move the F-actin/G-actin equilibrium toward F-actin. It returned to baseline level after washout of the NMDA, however, in contrast to the persistent change in the equilibrium induced by tetanus. This implies that NMDA receptor activation is necessary for the equilibrium change, but that for the shift to persist, an additional signal is also necessary.

An increase in phosphorylated cofilin in dentate gyrus LTP has been reported previously[10]. Moreover, phosphorylation of cofilin by the LIM domain–containing protein kinase (LIM-K) impairs its actin depolymerization activity[10]. In fact, a LIM-K knockout animal showed abnormal spine morphology and synaptic plasticity[46]. Small G-proteins located upstream of LIM-K are implicated in the maintenance of normal spine morphology[11]. The phosphorylated state of cofilin may be stabilized by a phosphoserine/threonine binding protein, 14-3-3, thereby stabilizing actin filaments[47]. On the other hand, the actin-stabilizing protein profilin is translocated to spine heads by activation of NMDA receptors[48], where it may contribute to stabilization of actin filaments. Involvement of gelsolin in the activity-dependent stabilization of actin has also been suggested[17].

Note added in proof: While this article was under revision, another group published a paper in Nature[51] *describing a similar expansion of dendritic spines accompanied by an increase in glutamate sensitivity.*

METHODS

Molecular biology and biochemistry. CFP- and YFP-actin were constructed by replacing EGFP in EGFP-actin (Clontech) with ECFP (Clontech) and an improved version of YFP (Venus)[49]. For spectrofluorometric assays, HEK293T cells were transfected with CFP- and YFP-actin at a ratio of 1:3, homogenized in a buffer containing 10 mM PIPES, 1 mM $MgCl_2$, 1 mM ATP and 0.5 mM DTT[27], and centrifuged at 3,000*g* for 1 min to clear large cell debris. This removed part of the F-actin to the pellet, resulting in a lower FRET signal than seen from imaging in intact cells.

Imaging in cell line. NIH3T3 cells were imaged with a custom-made two-photon laser scanning microscope in solution containing, in mM, NaCl 129; KCl 5; $CaCl_2$ 2; $MgCl_2$ 1; glucose 30; and sodium HEPES 25 (pH 7.4). The wavelengths used for FRET imaging were 800 nm (excitation), 480/30 nm (CFP emission) and 535/26 nm (YFP emission), separated by a 505 nm long-pass dichroic mirror. This combination allows leakage of the CFP signal into the YFP channel at about 31% efficiency. Because this leakage is purely optical and constant irrespective of FRET conditions, we did not correct for it. YFP did not leak into the CFP channel. Subsequently, the cells were fixed with 4% paraformaldehyde, stained with Texas Red–phalloidin and visualized at 900 nm (excitation) and 600/100 nm (emission).

Neuron imaging. Organotypic slice cultures of hippocampus were prepared as described in accordance with institutional guidelines[2]. The CA1 pyramidal neurons were biolistically cotransfected with CFP- and YFP-actin at a ratio of 1:3. The α and β isoforms of CaMKII were transfected at a ratio of 1:1 and CFP-actin and YFP-CaMKIIβ at a ratio of 1:3. Imaging was carried out 4–7 d after transfection in solution containing, in mM, NaCl 119; KCl 2.5; $CaCl_2$ 4; $MgCl_2$ 4; $NaHCO_3$ 26.2; NaH_2PO_4 1 and glucose 11, aerated with 95% O_2 and 5% CO_2. FRET imaging was carried out as above. YFP was imaged at 900 nm (excitation) and 535/26 nm (emission); GFP at 860 nm (excitation) and 570 nm short-pass (emission); and Alexa 594 at 800 nm (excitation) and 565 nm long-pass (emission). In the acceptor bleaching experiment, YFP was specifically photobleached at 525/45 nm for 1 min.

NMDA (2 μM) was applied in the presence of tetrodotoxin (1 μM) and Mg^{2+} (0.1 mM). For electrical stimulation, a glass electrode, filled with 1 M NaCl with fluorescent beads (1 μm) to allow visualization under fluorescence (~5 MΩ; A. Piccini, C. Kopec and R. Malinow, *Soc. Neurosci. Abstr.* 375.3, 2003), was placed within 5–15 μm of the dendrite. We and others confirmed that the tetanic stimulation at 100 Hz for 1 s given in this configuration provokes Ca^{2+}-response, LTP, insertion of AMPA receptors and generation of dendritic spines[2,5,7,50], whereas stimulation for 15 min at 1 Hz induces LTD and removal of AMPA receptors (A. Piccini, C. Kopec and R. Malinow, *Soc. Neurosci. Abstr.* 375.3, 2003). Phalloidin (100 μM) or Alexa 594 (20 μM) was injected through a whole-cell patch pipette filled with internal solutions containing, in mM, cesium methanesulfonate 115, CsCl 20, HEPES 10, $MgCl_2$ 2.5, adenosine triphosphate disodium salt 4, guanosine triphosphate trisodium salt 0.4, sodium phosphocreatine 10, and EGTA 0.6, at pH 7.25, under voltage clamp at –60 mV. For FRAP experiments, photobleaching was achieved by scanning a spine of interest at maximal excitation power (~1.4 W of pump laser output) for 5–10 times (~5 s).

Image analysis. The probability of stimulating multiple spines in a given dendritic segment was not high and the number of spines that responded to the stimulation varied significantly, most probably as a result of differences in the effectiveness of stimulation. We often moved the stimulation electrode, typically to a more proximal position (at least 100 μm away), before we found a number of spines that changed in response to the stimulation. We did not see any systematic difference in response among different levels of branches of apical dendrites. We analyzed dendritic segments on which >40% of spines showed changes in FRET level. We included all spines separated from dendrite shaft and adjacent spines.

For analyses, image stacks typically composed of 15–20 sections taken at 0.5-μm intervals were *z*-projected (summation), median-filtered and background-subtracted (Metamorph, Universal Imaging Corporation). The FRET images were displayed in intensity-modulated display mode, where warmer hue indicates a higher YFP/CFP ratio or FRET and the brightness indicates the intensity of the CFP channel.

FRET efficiency was calculated from the efficiency of dequenching of the CFP signal after specific photobleaching of the acceptor according to the formula:

$$\text{Efficiency} = \frac{F_{\text{CFP, after}} - F_{\text{CFP, before}}}{F_{\text{CFP, after}}}$$

where $F_{\text{CFP,before}}$ and $F_{\text{CFP,after}}$ represent the CFP signal before and after YFP bleaching.

The FRAP data were normalized by the baseline fluorescence and fitted to a single exponential curve using the following equation (Igor Pro, Wavemetrics):

$$F = F_{t=\infty} + A \exp\left(-\frac{t}{\tau}\right)$$

where $F_{t=\infty}$ represents unrecoverable fluorescence, considered to be a fixed population of fluorescent protein, and τ is the time constant for recovery.

To measure the spine width independently of the change in fluorescence, the CFP fluorescence profile was obtained along a line drawn across the middle of the dendritic spine perpendicular to the axis. In theory, the profile should be semielliptical, assuming that spine heads are spherical; but in most cases the profile was broadened owing to a convolution effect. In practice, therefore, we used a Gaussian fit (Origin, Microcal) to obtain the width as an index independent of the brightness of the structure, as follows:

$$F = F_{\text{background}} + F_{\text{peak}} \exp\left[-\frac{2(x-x_0)^2}{\text{width}^2}\right]$$

Here x is the position along the profile and x_0 is the peak position. The width represents twice the s.d. of the profile, corresponding to the half the width where fluorescence is 13.5% of the peak value (arrows in **Fig. 3e**). We confirmed that this measurement was independent of brightness by analyzing the same structure in the YFP channel, which, although it is weaker than the CFP channel, gave almost the same width.

Results are reported as mean ± s.e.m. and statistical significance was defined at $P < 0.05$. Statistical differences were determined using Wilcoxon tests except for **Figure 8**, where a nonpaired *t*-test was used.

ACKNOWLEDGMENTS

We thank K. Takao, H. Fujisawa, T. Kiuchi, E. Ruthazer, R. Malinow, M. Sheng, J. Lisman, F. Gertler, T. Emery and E. Hueske for valuable advice and sharing of resources. Y.H. is supported in part by The Ellison Medical Foundation.

COMPETING INTERESTS STATEMENT

The authors declare that they have no competing financial interest.

Received 17 May; accepted 7 July 2004
Published online at http://www.nature.com/natureneuroscience/

1. Sheng, M. & Pak, D.T. Ligand-gated ion channel interactions with cytoskeletal and signaling proteins. *Annu. Rev. Physiol.* **62**, 755–778 (2000).
2. Shi, S.H. *et al.* Rapid spine delivery and redistribution of AMPA receptors after synaptic NMDA receptor activation. *Science* **284**, 1811–1816 (1999).
3. Hayashi, Y. *et al.* Driving AMPA receptors into synapses by LTP and CaMKII: requirement for GluR1 and PDZ domain interaction. *Science* **287**, 2262–2267 (2000).
4. Shen, K., Teruel, M.N., Connor, J.H., Shenolikar, S. & Meyer, T. Molecular memory by reversible translocation of calcium/calmodulin-dependent protein kinase II. *Nat. Neurosci.* **3**, 881–886 (2000).
5. Piccini, A. & Malinow, R. Critical postsynaptic density 95/disc large/zonula occludens-1 interactions by glutamate receptor 1 (GluR1) and GluR2 required at different subcellular sites. *J. Neurosci.* **22**, 5387–5392 (2002).
6. Hosokawa, T., Rusakov, D.A., Bliss, T.V. & Fine, A. Repeated confocal imaging of individual dendritic spines in the living hippocampal slice: evidence for changes in length and orientation associated with chemically induced LTP. *J. Neurosci.* **15**, 5560–5573 (1995).
7. Maletic-Savatic, M., Malinow, R. & Svoboda, K. Rapid dendritic morphogenesis in CA1 hippocampal dendrites induced by synaptic activity. *Science* **283**, 1923–1927 (1999).
8. Engert, F. & Bonhoeffer, T. Dendritic spine changes associated with hippocampal long-term synaptic plasticity. *Nature* **399**, 66–70 (1999).
9. Buchs, P.A. & Muller, D. Induction of long-term potentiation is associated with major ultrastructural changes of activated synapses. *Proc. Natl. Acad. Sci. USA* **93**, 8040–8045 (1996).
10. Fukazawa, Y. *et al.* Hippocampal LTP is accompanied by enhanced F-actin content within the dendritic spine that is essential for late LTP maintenance in vivo. *Neuron* **38**, 447–460 (2003).
11. Lamprecht, R. & LeDoux, J. Structural plasticity and memory. *Nat. Rev. Neurosci.* **5**, 45–54 (2004).
12. Matus, A. Actin-based plasticity in dendritic spines. *Science* **290**, 754–758 (2000).
13. Rao, A. & Craig, A.M. Signaling between the actin cytoskeleton and the postsynaptic density of dendritic spines. *Hippocampus* **10**, 527–541 (2000).
14. Hering, H. & Sheng, M. Activity-dependent redistribution and essential role of cortactin in dendritic spine morphogenesis. *J. Neurosci.* **23**, 11759–11769 (2003).
15. Fischer, M., Kaech, S., Knutti, D. & Matus, A. Rapid actin-based plasticity in dendritic spines. *Neuron* **20**, 847–854 (1998).
16. Fifkova, E. & Morales, M. Actin matrix of dendritic spines, synaptic plasticity, and long-term potentiation. *Int. Rev. Cytol.* **139**, 267–307 (1992).
17. Star, E.N., Kwiatkowski, D.J. & Murthy, V.N. Rapid turnover of actin in dendritic spines and its regulation by activity. *Nat. Neurosci.* **5**, 239–246 (2002).
18. Halpain, S., Hipolito, A. & Saffer, L. Regulation of F-actin stability in dendritic spines by glutamate receptors and calcineurin. *J. Neurosci.* **18**, 9835–9844 (1998).
19. Capani, F., Martone, M.E., Deerinck, T.J. & Ellisman, M.H. Selective localization of high concentrations of F-actin in subpopulations of dendritic spines in rat central nervous system: a three-dimensional electron microscopic study. *J. Comp. Neurol.* **435**, 156–170 (2001).
20. Allison, D.W., Gelfand, V.I., Spector, I. & Craig, A.M. Role of actin in anchoring postsynaptic receptors in cultured hippocampal neurons: differential attachment of NMDA versus AMPA receptors. *J. Neurosci.* **18**, 2423–2436 (1998).
21. Zhou, Q., Xiao, M. & Nicoll, R.A. Contribution of cytoskeleton to the internalization of AMPA receptors. *Proc. Natl. Acad. Sci. USA* **98**, 1261–1266 (2001).
22. Colicos, M.A., Collins, B.E., Sailor, M.J. & Goda, Y. Remodeling of synaptic actin induced by photoconductive stimulation. *Cell* **107**, 605–616 (2001).
23. Kim, C.H. & Lisman, J.E. A role of actin filament in synaptic transmission and long-term potentiation. *J. Neurosci.* **19**, 4314–4324 (1999).
24. Krucker, T., Siggins, G.R. & Halpain, S. Dynamic actin filaments are required for stable long-term potentiation (LTP) in area CA1 of the hippocampus. *Proc. Natl. Acad. Sci. USA* **97**, 6856–6861 (2000).
25. Furuyashiki, T., Arakawa, Y., Takemoto-Kimura, S., Bito, H. & Narumiya, S. Multiple spatiotemporal modes of actin reorganization by NMDA receptors and voltage-gated Ca^{2+} channels. *Proc. Natl. Acad. Sci. USA* **99**, 14458–14463 (2002).
26. Furukawa, K. *et al.* The actin-severing protein gelsolin modulates calcium channel and NMDA receptor activities and vulnerability to excitotoxicity in hippocampal neurons. *J. Neurosci.* **17**, 8178–8186 (1997).
27. Wang, Y.L. & Taylor, D.L. Probing the dynamic equilibrium of actin polymerization by fluorescence energy transfer. *Cell* **27**, 429–436 (1981).
28. Miyawaki, A. *et al.* Fluorescent indicators for Ca^{2+} based on green fluorescent proteins and calmodulin. *Nature* **388**, 882–887 (1997).
29. Posern, G., Sotiropoulos, A. & Treisman, R. Mutant actins demonstrate a role for unpolymerized actin in control of transcription by serum response factor. *Mol. Biol. Cell* **13**, 4167–4178 (2002).
30. Kauer, J.A., Malenka, R.C. & Nicoll, R.A. NMDA application potentiates synaptic transmission in the hippocampus. *Nature* **334**, 250–252 (1988).
31. Petersen, C.C., Malenka, R.C., Nicoll, R.A. & Hopfield, J.J. All-or-none potentiation at CA3–CA1 synapses. *Proc. Natl. Acad. Sci. USA* **95**, 4732–4737 (1998).
32. Dunaevsky, A., Tashiro, A., Majewska, A., Mason, C. & Yuste, R. Developmental regulation of spine motility in the mammalian central nervous system. *Proc. Natl. Acad. Sci. USA* **96**, 13438–13443 (1999).
33. Shen, K., Teruel, M.N., Subramanian, K. & Meyer, T. CaMKIIβ functions as an F-actin targeting module that localizes CaMKIIα/β heterooligomers to dendritic spines. *Neuron* **21**, 593–606 (1998).
34. Sankaranarayanan, S., Atluri, P.P. & Ryan, T.A. Actin has a molecular scaffolding, not propulsive, role in presynaptic function. *Nat. Neurosci.* **6**, 127–135 (2003).
35. Bienenstock, E.L., Cooper, L.N. & Munro, P.W. Theory for the development of neuron selectivity: orientation specificity and binocular interaction in visual cortex. *J. Neurosci.* **2**, 32–48 (1982).
36. Bear, M.F. A synaptic basis for memory storage in the cerebral cortex. *Proc. Natl. Acad. Sci. USA* **93**, 13453–13459 (1996).
37. Nusser, Z. *et al.* Cell type and pathway dependence of synaptic AMPA receptor number and variability in the hippocampus. *Neuron* **21**, 545–559 (1998).
38. Harris, K.M. & Stevens, J.K. Dendritic spines of CA1 pyramidal cells in the rat hippocampus: serial electron microscopy with reference to their biophysical characteristics. *J. Neurosci.* **9**, 2982–2997 (1989).
39. Matsuzaki, M. *et al.* Dendritic spine geometry is critical for AMPA receptor expression in hippocampal CA1 pyramidal neurons. *Nat. Neurosci.* **4**, 1086–1092 (2001).
40. Lisman, J. & Goldring, M. Evaluation of a model of long-term memory based on the properties of the Ca^{2+}/calmodulin-dependent protein kinase. *J. Physiol. (Paris)* **83**, 187–197 (1988).
41. Malinow, R., Madison, D.V. & Tsien, R.W. Persistent protein kinase activity underlying long-term potentiation. *Nature* **335**, 820–824 (1988).
42. Esteban, J.A. *et al.* PKA phosphorylation of AMPA receptor subunits controls synaptic trafficking underlying plasticity. *Nat. Neurosci.* **6**, 136–143 (2003).
43. Frey, U. & Morris, R.G. Synaptic tagging and long-term potentiation. *Nature* **385**, 533–536 (1997).
44. Lee, S.H., Liu, L., Wang, Y.T. & Sheng, M. Clathrin adaptor AP2 and NSF interact with overlapping sites of GluR2 and play distinct roles in AMPA receptor trafficking and hippocampal LTD. *Neuron* **36**, 661–674 (2002).
45. Mulkey, R.M., Endo, S., Shenolikar, S. & Malenka, R.C. Involvement of a calcineurin/inhibitor-1 phosphatase cascade in hippocampal long-term depression. *Nature* **369**, 486–488 (1994).
46. Meng, Y. *et al.* Abnormal spine morphology and enhanced LTP in LIMK-1 knockout mice. *Neuron* **35**, 121–133 (2002).
47. Gohla, A. & Bokoch, G.M. 14–3-3 regulates actin dynamics by stabilizing phosphorylated cofilin. *Curr. Biol.* **12**, 1704–1710 (2002).
48. Ackermann, M. & Matus, A. Activity-induced targeting of profilin and stabilization of dendritic spine morphology. *Nat. Neurosci.* **6**, 1194–1200 (2003).
49. Nagai, T. *et al.* A variant of yellow fluorescent protein with fast and efficient maturation for cell-biological applications. *Nat. Biotechnol.* **20**, 87–90 (2002).
50. Mainen, Z.F., Malinow, R. & Svoboda, K. Synaptic calcium transients in single spines indicate that NMDA receptors are not saturated. *Nature* **399**, 151–155 (1999).
51. Matsukaski, M., Honkura, N., Ellis-Davies, G.C.R. & Kasai, H. Structural basis of long-term potentaation in single dedritic spines. *Nature* **429**, 761–766 (2004).